HHS Public Access

Author manuscript

Biomaterials. Author manuscript; available in PMC 2024 May 22.

Published in final edited form as:

Biomaterials. 2017 September ; 139: 229–243. doi:10.1016/j.biomaterials.2017.05.011.

Engineering a sprayable and elastic hydrogel adhesive with antimicrobial properties for wound healing

Nasim Annabi[a,b,c,*], **Devyesh Rana**[d,1], **Ehsan Shirzaei Sani**[a,1], **Roberto Portillo-Lara**[a,e], **Jessie L. Gifford**[d], **Mohammad M. Fares**[i], **Suzanne M. Mithieux**[f,g], **Anthony S. Weiss**[f,g,h]

[a]Department of Chemical Engineering, Northeastern University, Boston, MA, 02115, USA

[b]Biomaterials Innovation Center, Brigham and Women's Hospital, Harvard Medical School, Boston, MA, 02115, USA

[c]Harvard-MIT Division of Health Sciences and Technology, Massachusetts Institute of Technology, Cambridge, MA, 02139, USA

[d]Department of Bioengineering, Northeastern University, Boston, MA, 02115, USA

[e]Centro de Biotecnología FEMSA, Tecnológico de Monterrey, Monterrey, NL, 64700, Mexico

[f]School of Life and Environmental Sciences, Charles Perkins Centre, University of Sydney, NSW, Australia

[g]Charles Perkins Centre, University of Sydney, NSW, Australia

[h]Bosch Institute, University of Sydney, NSW, Australia

[i]Department of Chemical Sciences, Jordan University of Science & Technology, P.O. Box 3030, Irbid 22110, Jordan

Abstract

Hydrogel-based bioadhesives have emerged as alternatives for sutureless wound closure, since they can mimic the composition and physicochemical properties of the extracellular matrix. However, they are often associated with poor mechanical properties, low adhesion to native tissues, and lack of antimicrobial properties. Herein, a new sprayable, elastic, and biocompatible composite hydrogel, with broad-spectrum antimicrobial activity, for the treatment of chronic wounds is reported. The composite hydrogels were engineered using two ECM-derived biopolymers, gelatin methacryloyl (GelMA) and methacryloyl-substituted recombinant human tropoelastin (MeTro). MeTro/GelMA composite hydrogel adhesives were formed via visible light-induced crosslinking. Additionally, the antimicrobial peptide Tet213 was conjugated to

[*]Corresponding author. Department of Chemical Engineering, Northeastern University, Boston, MA 02115, USA. n.annabi@neu.edu (N. Annabi).

[1]These authors contributed equally

Author contribution statement

Idea and experimental design: NA; Performed the experiments and analyzed the data: DR, ESS, JG, and MF; Wrote, revised and corrected the paper: RPL, DR, ESS, SMM, ASW, and NA; All authors approved the final manuscript.

Competing financial interests

The authors declare no competing financial interests.

Appendix A. Supplementary data

Supplementary data related to this article can be found at http://dx.doi.org/10.1016/j.biomaterials.2017.05.011.

the hydrogels, instilling antimicrobial activity against Gram (+) and (−) bacteria. The physical properties (e.g. porosity, degradability, swellability, mechanical, and adhesive properties) of the engineered hydrogel could be fine-tuned by varying the ratio of MeTro/GelMA and the final polymer concentration. The hydrogels supported *in vitro* mammalian cellular growth in both two-dimensional and three dimensional cultures. The subcutaneous implantation of the hydrogels in rats confirmed their biocompatibility and biodegradation *in vivo*. The engineered MeTro/GelMA-Tet213 hydrogels can be used for sutureless wound closure strategies to prevent infection and promote healing of chronic wounds.

Keywords

Wound healing; MeTro; GelMA; Antimicrobial hydrogels; Tissue adhesive

1. Introduction

More than 2% of the US population suffers from chronic non-healing wounds, which represent an estimated 20 billion dollars in health care related costs each year [1]. Chronic wounds are characterized by delayed healing and sustained inflammation, as well as impaired extracellular matrix (ECM) function [2]. These wounds can be caused by a number of pathologies including diabetes mellitus, vascular insufficiency, local-pressure effects, compromised nutritional and immunological states, surgeries, and burns [3]. Conventional therapies for chronic wound management, such as skin substitutes or autologous skin grafts often fail to restore tissue homeostasis, and can lead to further health complications [3,4]. In particular, microbial infection at the wound site can severely prolong the healing process, lead to necrosis, sepsis, and even death [5]. Chronic wounds are highly susceptible to colonization by pathogenic bacteria such as *Escherichia coli, Pseudomonas aeruginosa, Staphylococcus aureus, Staphylococcus epidermis*, various filamentous fungi and yeasts (i.e. *Candida* spp.) [6–8]. Topical and systemic antibiotic administration is frequently prescribed to patients suffering from chronic wounds. However, the over-prescription, abuse, and misapplication of antibiotics have led to an escalating drug resistance in pathogenic microorganisms, which is associated with increased morbidity and mortality [9].

Polymeric hydrogels hold remarkable potential to be used as dressings for the treatment of non-healing wounds [5,6]. Hydrogels are hydrated three-dimensional (3D) networks of natural or synthetic polymers, which can be tailored to mimic the physicochemical properties of human tissues. Natural polymers that are derived from native ECM proteins such as collagen or elastin, are particularly advantageous for tissue-engineered wound dressings because of their inherent biocompatibility and biodegradability both *in vitro* and *in vivo* [10]. Hydrogel-based dressings also absorb wound exudates, which in turn promotes fibroblast proliferation, keratinocyte migration, and the eventual re-epithelialization of the wound [11]. Furthermore, wound healing and infection prevention can be promoted by delivering biomacromolecules, growth factors, and other small molecule agents via polymeric scaffolds [5,6]. In particular, previous works have demonstrated the incorporation of antimicrobial properties to hydrogel-based dressings through integration of different

types of biocidal agents, including metal nanoparticles [12,13], cationic polymers [14], and antimicrobial peptides (AMPs) [15].

Despite many biological advantages of hydrogel-based dressings, they often exhibit weak mechanical and adhesive properties on the wound area, when compared to conventional wound closure approaches (i.e. cyanoacrylate-based adhesives) [16]. Cyanoacrylates and aldehyde-based adhesives have been largely associated with tissue inflammation, cell necrosis, and cytotoxicity [17,18]. Hydrogel-based adhesives and biologically derived fibrin glues have been shown to exhibit poor adhesion to wet tissues, and are not able to support tissue regeneration [19]. In addition, poor mechanical properties and prolonged curing times of existing adhesives often lead to impaired performance and tissue bonding [20,21]. An ideal tissue adhesive for wound closure and treatment should be (i) biocompatible and biodegradable, (ii) rapidly cross-linked and easily applicable, (ii) antimicrobial and impervious to antibiotic resistance, (iii) strongly adhesive, (iv) tunable and long lasting, and (v) a promotor of tissue regeneration and wound healing [22,23]. Therefore, new biomaterial-based approaches are needed to address the limitations of currently available alternatives.

Here, we present a new composite class of elastic and antimicrobial hydrogels, for the clinical management of chronic non-healing wounds. The engineered hydrogels are comprised of two biopolymers derived from native ECM proteins, gelatin and tropoelastin. Both gelatin methacryloyl (GelMA) [24,25] and methacryloyl-substituted recombinant human tropoelastin (MeTro) [26,27] have been previously explored to engineer hydrogels through photocrosslinking using ultraviolet (UV) light. Although UV light has been extensively used for photocrosslinking of different biopolymers, it is also associated with DNA and tissue damage [28–31], adverse effects on cell metabolic activity [32], and suppression of the immune system *in vivo* [33]. Here, we describe for the first time the engineering of composite MeTro/GelMA hydrogels through visible light-mediated photocrosslinking. The use of a visible light-activated photoinitiator system eliminates the biosafety concerns associated with UV light, while yielding mechanical properties similar to, or comparatively better than UV-crosslinked hydrogels [34]. The physical, mechanical, and adhesive properties of the engineered MeTro/GelMA hydrogel adhesives were characterized. Additionally, to provide antimicrobial properties to the composite hydrogels, AMP Tet213 (KRWWKWWRRC) [35] was conjugated to the polymeric network. The antimicrobial properties of AMP incorporated MeTro/GelMA (MeTro/-AMP) hydrogels were evaluated against Gram-positive (G+) methicillin resistant *Staphylococcus aureus* (MRSA), and Gram-negative (G−) *E. coli*. Lastly, *in vitro* and *in vivo* cytocompatibility of optimized MeTro/GelMA-AMP hydrogels were investigated. The highly tunable mechanical and adhesive properties of MeTro/GelMA-AMP hydrogels showcase their potential for the engineering of multi-functional, biomaterial-based therapies for the treatment of chronic non-healing wounds.

2. Results and discussion

2.1. Synthesis and structural characterization of MeTro/GelMA hydrogels

In this study, we present a new composite class of elastic and antimicrobial hydrogels for the treatment of non-healing wounds. The engineered hydrogels were synthesized using MeTro and GelMA biopolymers, which mimic the native composition of the ECM. MeTro is a photocrosslinkable bioelastomer comprised of recombinant human tropoelastin, a highly elastic protein that provides structural integrity and modulates cell function in human tissues (Fig. 1a) [27]. On the other hand, GelMA is a photocrosslinkable biopolymer comprised of a modified form of denatured collagen, providing physiological cell binding motifs and protease-sensitive degradation sites (Fig. 1b) [36]. Due to their biocompatibility and high tunable mechanical properties, UV crosslinkable MeTro and GelMA biopolymers have been explored for various tissue engineering applications [24,26,27]. Here, we incorporated both MeTro and GelMA into a single polymeric network, enabling the modulation of several features of the resulting composite hydrogels such as degradation rate, mechanical properties, porosity, and tissue adhesion. In addition, we used a visible light activated photoinitiator system to minimize the biosafety concerns associated with UV light. Photopolymerizable scaffolds used for tissue engineering applications are generally crosslinked *in situ* using UV light (250 nm < λ < 400 nm). However, the exposure of living cells and tissues to UV radiation can induce DNA damage, leading to cell death and carcinogenesis [37]. To circumvent this limitation, we investigated a method of photocrosslinking of MeTro and GelMA through the use of visible light (400 nm < λ < 700 nm). Visible light is cheaper, safer, and possesses deeper tissue penetration for transdermal implantations, because of its longer wavelength [38,39]. In addition, similar to other photocrosslinking systems, the ability to control radical formation, makes this an ideal method for crosslinking. Visible light-induced crosslinking of MeTro/GelMA composite hydrogels was achieved through the incorporation of the type 2 initiator Eosin Y, with the co-initiator triethanolamine (TEA) and the co-monomer poly(N-vinylcaprolactam) (VC) (Fig. S1) to form an elastic and sprayable hydrogel for wound healing (Fig. 1c–d). This visible light mediated crosslinking scheme has been thoroughly investigated, showing improved cell viability when compared to UV crosslinked hydrogels [40–42]. Briefly, visible light excites dye molecules of Eosin Y into a triplet state, which abstracts hydrogen atoms from TEA. The deprotonated radicals initiate vinyl-bond crosslinking with VC via chain polymerization reactions, which leads to accelerated gelation [43]. The visible light photocrosslinking systems based on this chemistry, such as FocalSeal-L (Genyzme Biosurgery, Inc., Cambridge, MA), was approved by the Food and Drug Administration (FDA) [44].

To verify the degree of crosslinking within the hydrogels, ^{1}H NMR (500 MHz) spectra were taken from MeTro (Fig. 1e) and GelMA (Fig. 1f) prepolymers, and partially dissolved MeTro/GelMA-AMP crosslinked hydrogels (Fig. 1g). Results demonstrated that the methacrylated groups in the co-blended MeTro/GelMA-AMP network are involved in the formation of the 3D hydrogel network.Methacrylated groups (−C=CH_2) appeared as characteristic peaks corresponding to δ = 5.3 ppm (peak 1) and 5.7 ppm (peak 2), respectively (Fig. 1e–g). The extent of crosslinking was determined by the change in the

integrated areas of the peaks from the methacrylated groups after exposure to visible light. Using this approach, we determined that the degree of crosslinking was 87.1 ± 3.9%.

2.2. Mechanical properties of MeTro/GelMA hydrogels

Mechanical properties of MeTro/GelMA composite hydrogels were characterized through tensile and cyclic compression tests. Tensile tests on MeTro/GelMA hydrogels revealed that the elastic moduli (Fig. 2a) and extensibility (Fig. 2c) of the engineered hydrogels could be modulated by varying the MeTro/GelMA ratio and the total polymer concentration. Representative strain/stress curves for tensile and compression tests are shown in Fig. S2. The elastic moduli of composite hydrogels increased consistently from 4.05 ± 0.05 kPa to 18.35 ± 1.95 kPa (15% (w/v)), and from 10.25 ± 2.45 kPa to 32.2 ± 7.3 kPa (20% (w/v)) by changing the ratio of MeTro/GelMA from 100/0 to 0/100 (Fig. 2a). Although the elastic moduli of the engineered composite hydrogels were lower than that of native skin or epidermis (88 kPa – 300 kPa) [45], their elasticity was in the range of 11.7 ± 0.6% – 70.3 ± 6.6% which is close to the extensibility of the native skin (60–75%) [46]. It is expected that due to the excellent biological properties of the engineered hydrogels, cells from the surrounding tissues can infiltrate inside the gel and deposit autologous ECM components to form tissues with enhanced mechanical strength. The increased stiffness of the hydrogels at 20% polymer concentration is likely a result of the higher degree of crosslinking within the polymer network. Our results showed that hydrogels with a lower MeTro concentration exhibited a comparatively lower extensibility. This is likely due to the increased elasticity and enhanced recoverability of MeTro hydrogels [27]. Composite hydrogels synthesized with a 70/30 MeTro/GelMA ratio at 15% (w/v) polymer concentration, exhibited the highest extensibility (Fig. 2c). We hypothesize that at low concentrations, GelMA provides mechanical support to the backbone by its dispersion in the MeTro network. Steric hindrance caused by GelMA elongates the entire matrix, and changes the mechanical properties of the hydrogel by inhibiting certain MeTro crosslink sites [47]. For instance, it has been shown that GelMA at a low concentration (2% w/v) added to calcium phosphate cements (CPC), greatly enhances the physical properties of the entire composite, as compared to pure CPC or pure GelMA [48]. Hydrogels synthesized with 20% (w/v) polymer concentrations yielded a consistently higher ultimate stress as compared to lower concentration (15% (w/v)), except for 70/30 MeTro/GelMA hydrogels, where ultimate stress did not change significantly when increasing final polymer concentration (Fig. 2e). Compressive tests revealed similar tunability and control of compressive modulus (Fig. 2b) with minimal energy loss (Fig. 2d).

Lastly, we aimed to determine if incorporation of AMP could alter the mechanical properties of the composite scaffolds. Our findings demonstrated that the addition of AMP resulted in no significant changes in both elastic and compressive moduli, in 70/30 MeTro/GelMA hydrogels (Fig. 2f). These observations are likely due to the fact that the small size of AMP does not significantly alter the microarchitecture of the polymeric 3D network [49]. Taken together, these results demonstrated that MeTro/GelMA-AMP hydrogels could be tuned to possess high elasticity and low fatigue during continuous deformation, which is critical for hydrogel bioadhesives used for skin tissue regeneration.

2.3. Porosity, swellability and *in vitro* degradation of MeTro/GelMA hydrogels

Previous studies have investigated the influence of microstructural features of hydrogel scaffolds on the regeneration and repair of target tissues [50]. Here, we aimed to characterize the average pore size of MeTro/GelMA hydrogels, as well as their *in vitro* degradation and swellability. Scanning electron microscopy (SEM) images were acquired from lyophilized MeTro/GelMA hydrogels fabricated by using different ratios of MeTro to GelMA, at both 15% (w/v) (Fig. 3a) and 20% (w/v) (Fig. S3) polymer concentrations. Similar to the results of mechanical testing, the pore characteristics of the composite hydrogels were shown to be dependent on the MeTro/GelMA ratio and the final polymer concentration (Fig. 3b). Our results showed that the average pore sizes of the composite hydrogels increased from 26.85 ± 7.38 μm to 69.7 ± 11.23 μm at 15% (w/v) final polymer concentration, and from 10.9 ± 4.13 μm to 66.35 ± 13.92 μm at 20% (w/v) final polymer concentration by increasing the concentration of GelMA (Fig. 3b). Hydrogels at 15% (w/v) polymer concentration were shown to possess marginally larger pores, when compared to their 20% (w/v) counterparts. Although we observed some differences in the porosity of the engineered hydrogels formed by using different MeTro/GelMA ratios, it is important to note that the apparent porosity of these hydrogels could be affected due to the lyophilization prior to SEM analysis [50].

Swelling ratios of the composite hydrogels were also determined at various time points, throughout 24 h of incubation in DPBS at 37 °C. Our results demonstrated that hydrogels at 15% (w/v) (Fig. 3c) and 20% (w/v) (Fig. S4) polymer concentrations showed increasingly higher swelling ratios for hydrogel composition containing lower MeTro concentrations. 15% (w/v) hydrogels reached their maximum swelling ratios after 24 h, which corresponded to 10.5 ± 7.5% for 100/0 MeTro/GelMA hydrogel, 38.7 ± 3.8% for 70/30 MeTro/GelMA hydrogel, 95.5 ± 5.3% for 50/50 MeTro/GelMA hydrogel, 190.5 ± 10.1% for 30/70 MeTro/GelMA hydrogel, and 370 ± 16.2% for 0/100 MeTro/GelMA hydrogel (Fig. 3c). The wide range of swelling ratios obtained for MeTro/GelMA hydrogels is advantageous for tissue engineering applications since they could be finely tuned based on their final application. In addition, reduced swellability of composite hydrogels at higher MeTro concentrations could potentially enhance their adhesive properties *in vivo*. This is mainly due to their enhanced structural stability in physiological environments, long lasting tissue interactions, and sustained mechanical performance. For sutureless wound closure strategies, this could greatly enhance wound healing by providing a highly permeable and flexible seal. This further regulates elimination of exudates and production of ECM components that promote cellular function and tissue regeneration [51].

Another technical advantage of hydrogels used for sutureless wound closure is their controlled degradation in wet environments. Therefore, we aimed to investigate the *in vitro* degradation of 15% and 20% (w/v) MeTro/GelMA hydrogels in DPBS (Fig. S5) and DPBS supplemented with 10% fetal bovine serum (FBS) (Fig. 3d, and Fig. S5). Results demonstrated that the *in vitro* degradation rate of the composite hydrogels were dependent on MeTro/GelMA ratio and final polymer concentration. Overall, *in vitro* degradability was consistently higher at 50/50 MeTro/GelMA ratios for all conditions tested. Hydrogels incubated in DPBS/FBS exhibited greater degradability, when compared to incubation in DPBS. In addition, the incorporation of AMP resulted in no significant changes on the

degradability of the composite hydrogels (Fig. 3e). In contrast, previous studies have shown that the incorporation of antimicrobial agents such as ZnO in protein-based biopolymers, could significantly alter the degradation rate of the resulting biomaterials [52].

2.4. Adhesive properties of MeTro/GelMA hydrogels

Conventional wound closure methods, such as sutures, mechanical fasteners, and staples are often associated with increased localized stress, and tissue damage at the wound site. Thus, alternative strategies for sutureless wound closure could potentially simplify surgical procedures, and improve patient care and prognosis. In particular, tissue adhesives are associated with reduced trauma and pain, improved cosmetic outcome, and localized delivery of biocidal agents [53]. Therefore, we aimed to characterize the adhesive properties of MeTro/GelMA hydrogels, and compare them with those of commercially available tissue adhesives such as Evicel (Ethicon, Somerville, NJ, USA) and Coseal (Baxter, Deerfield, IL, USA). Lap shear, burst pressure, and wound closure tests were performed using standardized testing methodologies from the American Society for Testing and Materials (ASTM) [16,54,55].

Lap shear strength of composite hydrogels synthesized with different MeTro/GelMA ratios was calculated according to ASTM F2255-05 standard [54]. Shear adhesive strength of MeTro/GelMA hydrogels increased from 541.86 ± 69.9 kPa (100/0 MeTro/GelMA) to 1084.85 ± 104.64 kPa (0/100 MeTro/GelMA) at 15% (w/v) final polymer concentration, by increasing the concentration of GelMA (Fig. 4a). Our results also showed that increasing polymer concentration from 15% to 20% (w/v) significantly enhanced the adhesive properties of the resulting hydrogels. For example, the shear strength of 70/30 MeTro/GelMA hydrogels increased from 606.34 ± 96.2 kPa at 15% (w/v) to 803 ± 101 kPa at 20% (w/v) final polymer concentration (Fig. 4b). These values were significantly higher than those observed for both Evicel (207.65 ± 67.3 kPa) and Coseal (69.7 ± 20.6 kPa). As shown in Fig. 4b, the incorporation of AMP had no significant effect on the shear strength of 70/30 MeTro/GelMA produced at 15% polymer concentration.

Biomaterial-based dressings for non-healing wounds should also be able to withstand the pressure exerted by underlying tissues and fluids from within the wound site [56]. Therefore, burst pressure tests on the engineered composite hydrogels were conducted, based on a variation of the ASTM F2392-04 standard testing for surgical sealants [16,57]. The burst pressure for hydrogels at 15% (w/v) polymer concentration was ranged between 2.41 ± 1.3 kPa and 10.94 ± 2.84 kPa by changing MeTro/GelMA ratios (Fig. 4c). In addition, the burst pressure of 70/30 MeTro/GelMA hydrogels was also increased from 4.53 ± 1.32 kPa at 15% (w/v) to 6.84 ± 1.38 kPa at 20% (w/v) final polymer concentration. These values were also significantly higher than both Evicel (1.94 ± 0.99 kPa), and Coseal (1.68 ± 0.11 kPa), and very similar to 70/30 MeTro/GelMA hydrogels containing AMP (Fig. 4d).

Lastly, to characterize the ability of MeTro/GelMA hydrogels to seal wound boundaries upon tensile stress, we performed *in vitro* wound closure tests on native tissue, i.e. porcine skin, using ASTM F2458-05 standard [58]. The adhesion strength obtained for hydrogels at 15% (w/v) polymer concentration increased from 42.07 ± 2.6 kPa to 57.26 ± 5.68 kPa, by increasing the concentration of GelMA (Fig. 4e). The adhesive strength of 70/30

MeTro/GelMA hydrogels at 15% (w/v) (45.76 ± 2.64 kPa) and 20% (w/v) (46.24 ± 3.88 kPa) polymer concentration, was greater than those observed for Evicel (26.33 ± 4.67 kPa), and Coseal (19.38 ± 17.31 kPa) (Fig. 4f). Concurrently, the addition of AMP had no significant effect on the adhesive strength of 70/30 MeTro/GelMA produced at 15% polymer concentration.

These results together demonstrated tunable adhesive properties of MeTro/GelMA hydrogels and the applicability to different physiological scenarios. The engineered composite hydrogel adhesives offer several technical advantages over commercially available approaches, including their highly tunable nature, superior adhesive strength to native tissue, and increased resilience to burst pressure for adequate wound closure. In addition, the ability of GelMA to be enzymatically degraded could potentially foster tissue remodeling, while the elasticity of MeTro could provide mechanical support to the wound site. The strong adhesion properties of the engineered composite hydrogel can be attributed to hydrogel-tissue interlocking [59], covalent bonding with radicals generated during crosslinking [60], and hydrogen bonding in the presence of free hydroxyl groups within the hydrogel matrix [61].

2.5. *In vitro* antimicrobial properties of MeTro/GelMA-AMP hydrogels

In recent years, significant efforts have been made to develop macromolecular antimicrobial agents that are impervious to antibiotic resistance, and can be used in the context of chronic wound treatment [62]. AMPs are comprised of short sequences of cationic amino acids, which have been shown to possess broad-spectrum bactericidal activity against G(+/−) bacteria [63]. AMPs bind to the negatively charged outer leaflet of bacterial cell membranes, which leads to changes in bacterial surface electrostatics, actuation upon cytoplasmic targets, increased membrane permeabilization, and ultimately, cell lysis [6,64]. Here, we aimed to provide antimicrobial capabilities to the engineered MeTro/GelMA hydrogels through the incorporation of a broad spectrum AMP. We first investigated the kinetics of peptide release from MeTro/GelMA-AMP hydrogels. For this, 70/30 MeTro/GelMA hydrogels mixed with 0.1% (w/v) AMP were incubated in DPBS at 37 °C; and the amount of AMP released from the composite hydrogels was determined at 280 nm absorbance. MeTro/GelMA hydrogels were used as controls. Our results demonstrated that a burst release (~60%) of AMP from MeTro/GelMA hydrogels took place within the first 8 h post-incubation (Fig. 5a). After this, a relatively steady and sustained release of AMP (~80%) was observed for 72 h incubation. In contrast, previous studies have reported comparatively slower burst releases of AMPs from Carbopol® (35%) [65], and alginate sulfate (20%) [66] hydrogels at 48 h.

One possible reason for the initial burst release of AMP from the hydrogel network could be due to AMP diffusing out of the superficial layer of the hydrogel network, followed by a sustained release of AMP due to hydrogel swelling and degradation. This acute initial release of AMP from MeTro/GelMA-AMP hydrogels could potentially be advantageous in cases where colonization by pathogenic bacteria has already occurred. Furthermore, it is important to mention that the kinetics of the release should also be further investigated *in vivo* where the hydrogel is exposed to a physiological environment, instead of submerged in a solution. The modulation of the release profile of MeTro/GelMA-AMP hydrogels through

variations in the degree of crosslinking, biopolymer ratios, or concentrations could also be explored.

The antimicrobial activity of MeTro/GelMA-AMP hydrogels was evaluated using standard colony-forming unit (CFU) (Fig. 5b–c) and live/dead assays (Fig. 5d). We selected two model microorganisms that are associated with microbial colonization of chronic non-healing wounds, MRSA and *E. coli*. Composite hydrogels containing 0.1, 0.3% (w/v) AMP, or 3% (w/v) ZnO (control) were compared to hydrogels without ZnO and AMP. Hydrogels were incubated for 24 h in 1 mL of tryptic soy broth containing 10^6 CFU/ml of either MRSA or *E. coli*. After incubation, the hydrogels were harvested and processed for CFU and live/dead assays.

First, we used a CFU assay to evaluate the ability of the MeTro/GelMA-AMP hydrogels to prevent bacterial colonization. Hydrogels were washed three times with PBS and thoroughly vortexed to release bacteria from the scaffolds. Then, the resulting bacterial suspension was further diluted and used to seed tryptic soy agar plates. After 24 h of incubation, the number of colonies formed on each agar plate was counted. CFU assays demonstrated that MeTro/GelMA-AMP hydrogels were effectively protected from both MRSA and *E. coli* colonization, as shown by the reduction in CFU values when compared to MeTro/GelMA controls (Fig. 5b–c). Furthermore, no statistical significances were found between the hydrogels containing 0.1 and 0.3% (w/v) AMP, and those incorporated with 3% (w/v) ZnO (Fig. 5b–c and Fig. S6).

The antimicrobial ability of MeTro/GelMA-AMP hydrogels was further evaluated using Live/Dead BacLight Bacterial Viability Kit (Thermo Fisher Scientific). Hydrogels were harvested from bacterial cultures, as described above, and stained according to instructions from the manufacturer. Briefly, the green-fluorescent nucleic acid dye permeates the cell membrane of both live and dead bacteria cells. In contrast, the red-fluorescent propidium iodide permeates only through compromised cell membranes, while also quenching the green fluorescence in dead bacterial cells [67]. Our results showed that both MRSA and *E. coli* were able to infiltrate and effectively colonize on MeTro/GelMA hydrogels with no AMP, as demonstrated by the predominantly green fluorescence (Fig. 5d). In contrast, composite hydrogels containing 0.1 and 0.3% (w/v) AMP showed predominantly red fluorescence, which is indicative of dead bacterial cells. Similar to CFU assays, no observable differences were found between hydrogels with 0.1 and 0.3% (w/v) AMP. Furthermore, composite hydrogels incorporated with 3% (w/v) ZnO also showed a majority of red-fluorescent bacterial cells (Fig. 5d and Fig. S6).

The antimicrobial activity of ZnO nanoparticles and their potential applications for the development of wound healing approaches have been extensively reported in the literature [68,69]. However, recent studies have reported the adverse implications of ZnO nanoparticles in metal homeostasis [70] and cardiac function [71]. Interestingly, our results suggest that a qualitatively and quantitatively similar antimicrobial activity can be achieved using a concentration of AMP that is 30 times lower than that of ZnO nanoparticles (i.e., 0.1% (w/v) AMP vs. 3% (w/v) ZnO). Therefore, the use of peptide-based antimicrobial strategies provides a viable alternative that could help circumvent the known limitations

associated with ZnO, and aid in the engineering of safer approaches for the management of chronic wounds.

2.6. *In vitro* cytocompatibility of antimicrobial MeTro/GelMA hydrogels

To determine the cytocompatibility of the engineered composite hydrogels, we evaluated the *in vitro* viability, spreading, and metabolic activity of NIH-3T3 mouse embryonic fibroblast cells, using surface seeding (2D cultures) (Fig. S7) and 3D cell encapsulation (Fig. 6). Cell viability, spreading, and metabolic activity were determined using a commercial live/dead kit, Actin/DAPI staining, and PrestoBlue assays, respectively. 2D cell studies revealed that MeTro/GelMA hydrogels with 3% (w/v) ZnO resulted in lower cell viability and spreading when compared to MeTro/GelMA hydrogels with AMP and MeTro/GelMA hydrogels without AMP (controls) (Fig. S7). Cell viability in MeTro/GelMA-AMP hydrogels and controls remained >95%. The number of cells and their metabolic activity increased consistently until day 5 post-seeding (Fig. S7). Cell viability in hydrogels incorporated with 3% (w/v) ZnO remained < 65%, with cultures comprised of predominantly non-proliferating cells. Therefore, 3D cell encapsulation was carried out using only MeTro/GelMA-AMP hydrogels and MeTro/GelMA composites without AMP as controls.

3D encapsulation of 3T3 fibroblasts was performed using composite hydrogels (30/70 MeTro/GelMA ratio, 10% (w/v) final polymer concentration)with 0.1% (w/v) AMP and composite hydrogels without AMPs as controls (Fig. 6). Cell-laden MeTro/GelMA (Fig. 6a–b) and MeTro/GelMA-AMP (Fig. 6c–d) hydrogels were comprised of predominantly viable and proliferating cells over 5 days of culture. Similarly, Actin/DAPI staining revealed that 3T3 fibroblasts could proliferate and spread throughout MeTro/GelMA (Fig. 6e–f) and MeTro/GelMA-AMP (Fig. 6g–h) hydrogels. Furthermore, cell viability in MeTro/GelMA-AMP hydrogels and controls remained >85% (Fig. 6i), and the metabolic activity increased consistently until day 5 post encapsulation (Fig. 6j).

These results demonstrated that MeTro/GelMA-AMP hydrogels could support the proliferation and spreading of metabolically active cells *in vitro*, in both 2D and 3D culture systems. A recent study reported encapsulation and delivery of bone marrow-derived mesenchymal stem cells (BMSCs) in temperature sensitive hydrogels, to target the chronic inflammatory wound microenvironment [72]. This encapsulation of BMSCs into the hydrogel led to the inhibition of pro-inflammatory M1 macrophages and significantly greater contraction of wounds *in vivo*. However, this acrylamide-based hydrogel lacks the biological, antimicrobial, and highly tunable mechanical properties of MeTro/GelMA hydrogels. Therefore, the choice of MeTro/GelMA-AMP hydrogels could greatly enhance the effectiveness of stem cell-based therapies for chronic non-healing wounds.

2.7. *In vivo* biocompatibility and biodegradation of MeTro/GelMA hydrogels

Lastly, we characterized the *in vivo* biodegradation of MeTro/GelMA-AMP hydrogels, including their interaction with native tissues via subcutaneous implantation in a murine animal model. Composite hydrogels (30/70 MeTro/GelMA ratio, 15% (w/v) final polymer concentration) were implanted in subcutaneous pockets, prepared along the dorsomedial skin of male Wistar rats. At days 4, 14, 28, and 56 post-implantation, animals were

euthanized prior to hydrogel retrieval, along with the adjacent tissues. Our results revealed sustained biodegradation, as demonstrated by visual inspection (Fig. 7a) and changes in the percentage of both weight and volume (Fig. 7b) of the explanted hydrogels. Explanted samples were then flash-frozen in an optimal cutting temperature (OCT) compound, cryosectioned into 14-μm slices, and mounted in glass slides for histological examination. Hematoxylin and eosin (H&E) staining of the explanted samples revealed that biodegradation of MeTro/GelMA-AMP hydrogels enabled ingrowth of predominantly non-inflammatory cells and the almost complete replacement of the hydrogel with autologous tissue (Fig. 7c–e). These results confirmed that composite hydrogels could be efficiently biodegraded *in vivo*, through the enzymatic hydrolysis of the bio-polymeric scaffold.

Cryosectioned samples were also analyzed through immunohistofluorescent staining of leukocyte and macrophage antigens, CD3 and CD68, respectively. Fluorescence images revealed negligible leukocyte infiltration throughout the duration of the experiment, as demonstrated by the absence of the red-fluorescent CD3 antigen (Fig. 7f–h). In contrast, macrophage infiltration was observed at day 4 post-implantation, as demonstrated by the red-fluorescent CD68 antigen (Fig. 7i). However, this response was not sustained after day 28 (Fig. 7j–k). Therefore, this acute inflammatory response may be associated with the surgical procedure used to deliver the samples to the subcutaneous pockets, and is not associated with the material itself.

These results showcase the high degree of biodegradation and *in vivo* biocompatibility of MeTro/GelMA-AMP hydrogels. The rate of degradation for protein-based polymeric hydrogels has been shown to be modulated by variations in the concentrations of the biopolymers. Therefore, it is possible to finely-tune the amount of time that the hydrogels will remain associated with tissues to ensure proper mechanical support and antimicrobial protection to the wound site. Complex physiological responses could be elicited through the biological activities of the biopolymers. For example, previous studies have demonstrated the induction of angiogenic responses by GelMA [73] and tropoelastin-based [74] biomaterials. Furthermore, the incorporation of different types of immunomodulators, such as corticosteroids, nonsteroidal anti-inflammatory drugs (NSAIDs), or small interfering RNAs (siRNAs), could be further explored to modulate tissue responses at the wound site [75].

3. Conclusion

In this work, we introduce a new class of multi-functional hydrogel adhesives for the treatment of chronic non-healing wounds. Composite hydrogels were synthesized from two naturally derived biopolymers, MeTro and GelMA. The synergistic association of two biopolymers with distinct physicochemical properties enabled fine-tuning of various properties of the composite hydrogels including mechanical properties, *in vitro* and *in vivo* degradation, swellability, and porosity. The adhesive properties of the composite hydrogels were shown to be readily tunable to different physiological scenarios and comparatively superior to commercially available tissue adhesives. Incorporation of an antimicrobial peptide to the hydrogel network provided a wide-spectrum antibacterial properties to MeTro/GelMA-AMP hydrogels, which was significantly more potent than ZnO nanoparticles.

MeTro/GelMA-AMP hydrogels were shown to support the growth, spread, and proliferation of both, 2D surface seeded and 3D encapsulated fibroblasts *in vitro*. Furthermore, MeTro/GelMA-AMP hydrogels elicited minimal inflammatory responses, and were shown to be efficiently biodegraded *in vivo* when implanted subcutaneously in a murine animal model. Taken together, our results demonstrate the remarkable potential of MeTro/GelMA-AMP hydrogels for the engineering of sutureless regenerative and antimicrobial hydrogel adhesives, which could prevent infection and promote healing of chronic wounds.

4. Experimental section

4.1. Synthesis of MeTro/GelMA hydrogels

MeTro [27] and GelMA [36] biopolymers were synthesized as described elsewhere. Lyophilized biopolymers were dissolved in a solution containing TEA (1.8% w/v) and VC (1.25% w/v) in distilled water. MeTro was diluted and kept at 4 °C prior to crosslinking to prevent coacervation and aggregation of the biopolymer whereas GelMA was held at room temperature. Eosin Y disodium salt (0.5 mM) was dissolved separately in distilled water. The biopolymers/TEA/VC solution was mixed with Eosin Y, and 70 μL of the final solution was placed into polydimethylsiloxane (PDMS) cylindrical (diameter: 6 mm; height: 2.5 mm) molds for compressive tests, or rectangular (14 × 5 × 1 mm) molds for tensile tests. The resulting solution was photocrosslinked via exposure to visible light (450–550 nm) for 160 s, using a LS1000 FocalSeal Xenon Light Source (Genzyme). Composite hydrogels were synthesized using five MeTro/GelMA ratios (i.e., 100/0, 70/30, 50/50, 30/70, and 0/100), and 2 total polymer concentrations (i.e., 15% (w/v), and 20% (w/v)). Prior to experimentation, hydrogels were incubated in DPBS for 30 min to remove any unreacted Eosin Y.

MeTro/GelMA-AMP hydrogels were formed by dispersing 1 and 3 mg of AMP Tet213 (CSCScientific, Inc.) with TEA (1.8% (w/v)) and VC (1.25% (w/v)) in 1 mL distilled water. The lyophilized biopolymers were dissolved in the AMP/TEA/VC solution, and the complete hydrogel precursor solutions were then photocrosslinked as described previously.

MeTro/GelMA-ZnO hydrogels were formed by dispersing 3% (w/v) ZnO (US Research Nanomaterials, Inc.; 60–120 nm), 1.8% (w/v) TEA, and 1.25% (w/v) VC in distilled water. The lyophilized biopolymers were dissolved in the ZnO/TEA/VC solution, and mixed with Eosin Y. Following this, 70 μL of the complete hydrogel precursor solutions were pipetted into PDMS molds as required, and photocrosslinked as described previously.

4.2. ^{1}H NMR characterization of MeTro/GelMA hydrogels

^{1}H NMR analysis was conducted to calculate the degree of crosslinking within the polymer network using a Varian Inova-500 NMR spectrometer. ^{1}H NMR spectra were acquired from MeTro (15% (w/v)) and GelMA (15% (w/v)) prepolymers dissolved in deuterium oxide (D_2O). MeTro/GelMA-AMP crosslinked hydrogels (70/30 MeTro to GelMA ratio, 0.1% AMP, and 15% (w/v) final polymer concentration) were first partially dissolved overnight under agitation in deuterated dimethyl sulfoxide (DMSO-d_6). ^{1}H NMR spectra were then acquired from the supernatant as described previously in the literature [76]. Peak values of

δ = 5.3 and 5.7 ppm were correlated to the presence of methacrylated groups. The extent of crosslinking was calculated from the change in peak area for the double bond groups $\left(-\frac{\partial(C=C)}{\partial t}\right)$ within the time of exposure to visible light (120 s), using the following formula: [76]

$$Extent\ of\ Crosslinking\,(\%) = \left(\frac{PA_b - PA_a}{PA_b}\right) \times 100 \quad (1)$$

where $\boldsymbol{PA_b}$ and $\boldsymbol{PA_a}$ corresponds to the peak areas before and after exposure to visible light, respectively, and are the concentration of bonds participating in the crosslinking process. Peak areas were integrated with respect to phenyl conjugated peaks at δ = 6.5–7.5 ppm, using ACD/Spectrus NMR analysis software.

4.3. Characterization of the mechanical properties

After photocrosslinking, hydrogels were incubated for 1 h in DPBS. The subsequent swollen gels were measured using digital calipers. Uniaxial tensile test and cyclic uniaxial compression test were conducted using an Instron 5542 mechanical tester. Hydrogels for tensile testing were placed between two pieces of double sided tape within tension grips of the instrument, and extended at a rate of 1 mm/min until failure. Elastic moduli were calculated by obtaining the slope of the stress-strain curves. Hydrogels for compressive testing were loaded onto compression plates of the instrument under wet conditions, by submerging the plates in a DPBS bath. Cyclic uniaxial compression tests were conducted at a 90% strain level and 1 mm/min strain rate. Hydrogels were conditioned cyclically (loading and unloading) for 7 cycles. Post-preconditioning, the hydrogel underwent a final cycle. Compressive strain (mm) and load (N) were then measured at the 8th cycle using an Instron's Bluehill 3 software. Moduli were determined by obtaining the tangent of the slope of the linear region on the loading stress/strain curve. Energy loss was calculated by obtaining the area between the loading and unloading curves (n = 5).

4.4. *In vitro* lap shear test

Shear strength of the composite hydrogels, as well as other commercial tissue adhesives, such as Evicel and Coseal was tested according to the modified ASTM F2255-05 standard for tissue adhesives [54]. Two pieces of 2 cm × 1 cm were cut from a glass slide. A 1 cm × 1 cm layer of gelatin was formed onto each piece of glass slide, and left to dry to function as a base layer. The remaining 1 cm × 1 cm uncoated area was covered by a tape, which was later used to clamp the glass slides into the Instron machine. A 10 μL drop of hydrogel precursor solution was crosslinked between the two layers of gelatin coated glass slides. The two glass slides were placed in the mechanical tester, and tensile loading was applied with a strain rate of 10 mm/min. Shear strength was calculated at the point of detaching (n = 5).

4.5. *In vitro* burst pressure test

Burst pressure of composite hydrogels, Evicel, and Coseal was calculated by using the ASTM F2392-04 standard [57]. Porcine intestine was obtained from a local butcher.

Intestine was placed in between two stainless steel annuli from a custom built burst-pressure apparatus, which consists of a metallic base holder, pressure meter, syringe pressure setup, and data collector. A pinsized hole puncture was made through the intestine and air was flowed using a syringe pump at 0.5 ml/s. The hole made on the intestine was covered with a crosslinked hydrogel, prior to initiating the pump and sensor. Airflow was terminated post hydrogel rupture and the burst strength (pressure) was recorded (n = 5).

4.6. *In vitro* wound closure test

Wound closure of the composite hydrogels, Evicel, and Coseal was calculated by using the ASTM F2458-05 standard [58]. Porcine skin was obtained from a local butcher and cut into small strips (1 ×2 cm), with excess fat was removed. Tissues were immersed into PBS before testing to prevent drying in the air. The tissues were fixed onto two pre-cut poly(methyl methacrylate) slides (20 mm × 60 mm) by ethyl 2-cyanoacrylate glue (Krazy glue; Westerville, OH, USA). 6 mm spaces was kept between the slides using the porcine skin. The tissue was then separated in the middle with a straight edge razor to simulate the wound. 100 μL of polymer solution was administered onto the desired adhesive area and crosslinked by light. Maximum adhesive strength of each sample was obtained at the point of tearing at strain rate of 1 mm/min using a mechanical tester (n = 5).

4.7. Scanning electron microscope (SEM) analysis

SEM imaging and analysis were conducted to evaluate the porosity of the crosslinked composite hydrogels. Lyophilized hydrogel samples were prepared using the compressive molds described earlier. SEM images were obtained using a Hitachi S-4800 Scanning Electron Microscope (SEM). Pore sizes of MeTro/GelMA hydrogels were averaged from at least 3 images from 3 samples for each condition by using ImageJ software (n = 5).

4.8. Evaluation of *in vitro* swelling ratio and degradation

Swellability of MeTro/GelMA scaffolds was determined by incubating the composite hydrogels in DPBS at 37 °C for 24 h. MeTro/GelMA hydrogels were prepared as described previously for compression testing. Samples were then lyophilized, and their dried weights were measured. Changes in mass were recorded throughout a 24 h incubation period in DPBS. Swelling ratio was defined by the ratio of final weight to initial dry weight.

To evaluate the degree of *in vitro* degradation, hydrogels were freeze-dried, weighed, and placed in 24-well plate with 1 ml of DPBS or DPBS + FBS solutions at 37 °C for 2 weeks. The DPBS/FBS solutions were refreshed every 3 days. At days 1, 7 and 14 post-incubation the samples were freeze-dried and weighed (n = 5).

4.9. Antimicrobial peptide (Tet213) release studies

In vitro peptide release profile was obtained using UV/Vis spectroscopy. Absorbance was measured at 280 nm, which corresponds to an excitation wavelength of tryptophan. A series of AMP dilutions were prepared in DPBS (2–100 μg/ml) in order to construct the calibration curve used to determine the AMP release kinetics. Composite hydrogels containing AMP (0.1% w/v) were used for the release study. AMP incorporated hydrogels were prepared and then incubated in microcentrifuge tubes with 1 mL DPBS at 37 °C. After this, 500 μl of

the solution was taken from each tube at different time points (i.e., 30 min, 60 min, 120 min, 240 min, 560 min, 1 day, 2 days, and 3 days). Finally, the AMP concentration in each sample was measured using UV/Vis spectroscopy, and the cumulative AMP release was calculated.

4.10. *In vitro* evaluation of antimicrobial activity

Hydrogels with AMP (0.1% and 0.3% w/v), and ZnO (3% w/v), were prepared as described previously using a compressive mold. Next, MeTro/GelMA hydrogels containing AMP or ZnO were deposited into a 24 well plate, in separate wells, and sterilized under UV light. Gram-positive Methicillin Resistant *Staphylococcus aureus* (MRSA) and Gram-negative *E. coli* (ATCC 25922) were used as models to evaluate the antimicrobial properties of the composite hydrogels. A single colony of each strain of bacteria was mixed in tryptic soy broth (TSB; Sigma-Aldrich; 5 mL), and incubated overnight in a bacterial shaker incubator (200 rpm at 37 °C). The optical density (OD) of the resulting bacterial suspension was adjusted to an OD of 0.52 (10^9 CFU/ml) at a wavelength of 570 nm using a spectrophotometer. This suspension was then serially diluted to a density of 10^6 CFU/ml. Subsequently, 1 ml of the bacterial suspension was added directly to each hydrogel. The well plate was subsequently incubated in a bacterial incubator at 37 °C and 5% CO_2 for 24 h. After incubation, scaffolds were carefully washed 3 times with PBS to remove excess bacteria. For CFU assays, hydrogels were placed in 1 ml PBS in microcentrifuge tubes, which were then vigorously vortexed at 3000 rpm for 15 min. The vortex propagates the release of bacteria from the scaffold into the solution. Each bacterial suspension was serially diluted in PBS over 3 logarithmic dilutions in a 96 well plate. Three 20-μL drops of each dilution were seeded on agar (which includes TSB media) plates, which were then incubated for 24 h at 37 °C and 5% CO_2. Lastly, the number of bacterial colonies formed on each agar plate was counted, and the dilution factor was used to calculate CFU values. For bacterial viability assays, hydrogels incubated in bacterial tryptic soy broth were harvested as described previously. After washing, a commercial LIVE/DEAD® BacLight™ kit (ThermoFisher Scientific) was used to determine bacterial cell viability, according to instructions from the manufacturer. Fluorescently stained samples were imaged via a Zeiss Axio Observer Z1 inverted microscope.

4.11. Two-dimensional (2D) surface cell seeding

NIH 3T3 cells were cultured at 37 °C and 5% CO_2 in Dulbecco's Modified Eagle Medium (DMEM) media (Gibco), supplemented with FBS (10% v/v) and penicillin/streptomycin (1% v/v). 70/30 MeTro/GelMA hydrogels at 15% (w/v) polymer concentrations were used for 2D cultures. Hydrogels were formed by pipetting 7 μl of precursor solution onto 3-(trimethoxysilyl) propyl methacrylate (TMSPMA, Sigma-Aldrich) coated glass slides separated by 100 μm spacers. After photocrosslinking, 3T3 cells (5×10^6 cells/ml) were seeded on the hydrogel. 2D cultures were maintained at 37 °C, 5% CO_2, and humidified atmosphere.

4.12. Three-dimensional (3D) cell encapsulation

For 3D cell encapsulation, precursor hydrogel solutions were prepared in cell culture media containing TEA (1.8% w/v) and VC (1.25% w/v), and gently mixed with 3T3 cells (5×10^5

cells/ml). A single 7 μl-drop of this mixture was pipetted on a 150 μm spacer, and covered by a TMSPMA-coated glass slide. After photocrosslinking, the hydrogels were washed several times with warm media to remove the unreacted photoinitiators. The cell-laden gels were then placed in 24 well plates and incubated at 37 °C, 5% CO_2, and humidified atmosphere.

4.13. Cell viability and proliferation assays

Cell viability was determined via a Calcein AM/ethidium homodimer-1 live/dead kit (Invitrogen) according to instructions from the manufacturer. The experiments were carried out on days 1, 3 and 5 post-seeding. Fluorescence images were acquired using a Zeiss Axio Observer Z1 inverted microscope and analyzed using ImageJ software. Percent viability was determined as the ratio of viable cells to total number of cells. PrestoBlue cell viability kit (Thermo Fisher Scientific) was used to evaluate metabolic activity (MA) of cells, according to manufacturer protocol. MA was evaluated on days 0, 1, 3, and 5 post-seeding. Fluorescence intensity of the resulting solutions was recorded at 535–560 nm excitation and 590–615 nm emission.

4.14. Subcutaneous implantation

All animal experiments were reviewed and approved by Institutional Animal Care and Use Committee (ICAUC; protocol 15–1248R) at Northeastern University (Boston, MA, USA). Male Wistar rats (200–250 g) were obtained from Charles River (Boston, MA, USA) and housed in the local animal care facility under conditions of circadian day-night rhythm and feeding *ad libitum*. Anesthesia was achieved by isoflurane (2.5%) inhalation, followed by SC buprenorphine (0.02–0.05 mg/kg) administration. After inducing anesthesia, eight 1-cm incisions were made on the posterior dorsomedial skin, and small lateral subcutaneous pockets were prepared by blunt dissection.

Composite hydrogels (30/70 MeTro/GelMA ratio, 15% (w/v) final polymer concentration) were formed using cylindrical compression molds as described previously. The hydrogels were lyophilized, weighed, measured with digital calipers, and sterilized. The dried sterile hydrogels were then implanted in subcutaneous pockets along the dorsomedial skin of male Wistar rats. At days 4, 14, 28, and 56 post-implantation, animals were euthanized and the hydrogels were retrieved along with the surrounding tissues for histological assessment, and placed in cold DPBS. Hydrogels used for biodegradation studies were thoroughly washed in distilled water, and excess tissue was carefully removed under a dissection microscope.

4.15. Histological analysis and immunofluorescent staining

After explantation, samples were fixed in paraformaldehyde (4% v/v)) for 4 h, followed by overnight incubation in 30% sucrose (30% w/v) at 4 °C. Samples were then embedded in OCT and flash frozen in liquid nitrogen. Frozen samples were sectioned using a Leica Biosystems CM3050 S Research Cryostat. 14-μm cryosections were obtained and mounted in positively charged slides using DPX mountant medium (Sigma). Slides were then processed for hematoxylin and eosin staining (Sigma) according to instructions from the manufacturer. Immunohistofluorescent staining was performed on mounted cryosections as previously reported [77]. Anti-CD3 [SP7] (ab16669) and anti-CD68 (ab125212)

(Abcam) were used as primary antibodies, and an Alexa Fluor 594-conjugated secondary antibody (Invitrogen) was used for detection. All sections were counterstained with DAPI (Invitrogen), and visualized on an AxioObserver Z1 inverted microscope.

4.16. Statistical analysis

Data analysis was carried out using a 2-way ANOVA test with GraphPad Prism 6.0 software. Error bars represent mean ± standard deviation (SD) of measurements (*$p < 0.05$, **$p < 0.01$, and ***$p < 0.001$).

Supplementary Material

Refer to Web version on PubMed Central for supplementary material.

Acknowledgements

N.A. acknowledges support from the FY17 TIER 1 Interdisciplinary Research Seed Grants, Northeastern University, startup funds provided by the Department of Chemical Engineering, College of Engineering at Northeastern University, and the support from the American Heart Association (AHA, 16SDG31280010). A.S.W. acknowledges funding from Australian Research Council and National Health & Medical Research Council. A.S.W. is the Scientific Founder of Elastagen Pty Ltd.

References

[1]. Frykberg RG, Banks J, Challenges in the treatment of chronic wounds, Adv. Wound Care (New Rochelle) 4 (9) (2015) 560–582. [PubMed: 26339534]

[2]. Humphreys G, Lee GL, Percival SL, McBain AJ, Combinatorial activities of ionic silver and sodium hexametaphosphate against microorganisms associated with chronic wounds, J. Antimicrob. Chemother 66 (11) (2011) 255–2561.

[3]. Werdin F, Tenenhaus M, Rennekampff HO, Chronic wound care, Lancet 372 (9653) (2008) 1860–1862. [PubMed: 19041788]

[4]. Ammons MCB, Ward LS, James GA, Anti-biofilm efficacy of a lactoferrin/xylitol wound hydrogel used in combination with silver wound dressings, Int. Wound J 8 (3) (2011) 268–273. [PubMed: 21457463]

[5]. Ng VW, Chan JM, Sardon H, Ono RJ, Garcia JM, Yang YY, Hedrick JL, Antimicrobial hydrogels: a new weapon in the arsenal against multidrug-resistant infections, Adv. Drug Deliv. Rev 78 (2014) 46–62. [PubMed: 25450263]

[6]. Veiga AS, Schneider JP, Antimicrobial hydrogels for the treatment of infection, Biopolymers 100 (6) (2013) 637–644. [PubMed: 24122459]

[7]. Kalan L, Loesche M, Hodkinson BP, Heilmann K, Ruthel G, Gardner SE, Grice EA, Redefining the chronic-wound microbiome: fungal communities are prevalent, dynamic, and associated with delayed healing, MBio 7 (5) (2016).

[8]. Edwards R, Harding KG, Bacteria and wound healing, Curr. Opin. Infect. Dis 17 (2) (2004) 91–96. [PubMed: 15021046]

[9]. Frieri M, Kumar K, Boutin A, Antibiotic resistance J Infect. Public Health (2016).

[10]. Zhao L, Li X, Zhao J, Ma S, Ma X, Fan D, Zhu C, Liu Y, A novel smart injectable hydrogel prepared by microbial transglutaminase and human-like collagen: its characterization and biocompatibility, Mater Sci. Eng. C Mater Biol. Appl 68 (2016) 317–326. [PubMed: 27524026]

[11]. Xiao Y, Reis LA, Feric N, Knee EJ, Gu J, Cao S, Laschinger C, Londono C, Antolovich J, McGuigan AP, Radisic M, Diabetic wound regeneration using peptide-modified hydrogels to target re-epithelialization, Proc. Natl. Acad. Sci. U. S. A 113 (40) (2016) E5792–E5801. [PubMed: 27647919]

[12]. Hajipour MJ, Fromm KM, Ashkarran AA, Jimenez de Aberasturi D, de Larramendi IR, Rojo T, Serpooshan V, Parak WJ, Mahmoudi M, Antibacterial properties of nanoparticles, Trends Biotechnol. 30 (10) (2012) 499–511. [PubMed: 22884769]

[13]. Palza H, Antimicrobial polymers with metal nanoparticles, Int. J. Mol. Sci 16 (1) (2015) 2099–2116. [PubMed: 25607734]

[14]. Munoz-Bonilla A, Fernandez-Garcia M, Polymeric materials with antimicrobial activity, Prog. Polym. Sci 37 (2) (2012) 281–339.

[15]. Ageitos JM, Sanchez-Perez A, Calo-Mata P, Villa TG, Antimicrobial peptides (AMPs): ancient compounds that represent novel weapons in the fight against bacteria, Biochem. Pharmacol 133 (2016) 117–138. [PubMed: 27663838]

[16]. Ghobril C, Grinstaff MW, The chemistry and engineering of polymeric hydrogel adhesives for wound closure: a tutorial, Chem. Soc. Rev 44 (7) (2015) 1820–1835. [PubMed: 25649260]

[17]. Tseng YC, Tabata Y, Hyon SH, Ikada Y, In vitro toxicity test of 2-cyanoacrylate polymers by cell culture method, J. Biomed. Mater Res 24 (10) (1990) 1355–1367. [PubMed: 2283353]

[18]. Dong RH, Qin CC, Qiu X, Yan X, Yu M, Cui L, Zhou Y, Zhang HD, Jiang XY, Long YZ, In situ precision electrospinning as an effective delivery technique for cyanoacrylate medical glue with high efficiency and low toxicity, Nanoscale 7 (46) (2015) 19468–19475. [PubMed: 26531687]

[19]. Sierra DH, Eberhardt AW, Lemons JE, Failure characteristics of multiple-component fibrin-based adhesives, J. Biomed. Mater Res 59 (1) (2002) 1–11. [PubMed: 11745531]

[20]. Taguchi T, Saito H, Uchida Y, Sakane M, Kobayashi H, Kataoka K, Tanaka J, Bonding of soft tissues using a novel acid derivative tissue adhesive consisting of a citric and collagen, Mat. Sci. Eng. C-Bio S 24 (6–8) (2004) 775–780.

[21]. Jeon EY, Hwang BH, Yang YJ, Kim BJ, Choi BH, Jung GY, Cha HJ, Rapidly light-activated surgical protein glue inspired by mussel adhesion and insect structural crosslinking, Biomaterials 67 (2015) 11–19. [PubMed: 26197411]

[22]. Mehdizadeh M, Yang J, Design strategies and applications of tissue bioadhesives, Macromol. Biosci 13 (3) (2013) 271–288. [PubMed: 23225776]

[23]. Annabi N, Yue K, Tamayol A, Khademhosseini A, Elastic sealants for surgical applications, Eur. J. Pharm. Biopharm 95 (Pt A) (2015) 27–39. [PubMed: 26079524]

[24]. Yue K, Trujillo-de Santiago G, Alvarez MM, Tamayol A, Annabi N, Khademhosseini A, Synthesis, properties, and biomedical applications of gelatin methacryloyl (GelMA) hydrogels, Biomaterials 73 (2015) 254–271. [PubMed: 26414409]

[25]. Klotz BJ, Gawlitta D, Rosenberg AJ, Malda J, Melchels FP, Gelatin-methacryloyl hydrogels: towards biofabrication-based tissue repair, Trends Biotechnol. 34 (5) (2016) 394–407. [PubMed: 26867787]

[26]. Annabi N, Tsang K, Mithieux SM, Nikkhah M, Ameri A, Khademhosseini A, Weiss AS, Highly elastic micropatterned hydrogel for engineering functional cardiac tissue, Adv. Funct. Mater 23 (39) (2013).

[27]. Annabi N, Mithieux SM, Zorlutuna P, Camci-Unal G, Weiss AS, Khademhosseini A, Engineered cell-laden human protein-based elastomer, Biomaterials 34 (22) (2013) 5496–5505. [PubMed: 23639533]

[28]. Kielbassa C, Roza L, Epe B, Wavelength dependence of oxidative DNA damage induced by UV and visible light, Carcinogenesis 18 (4) (1997) 811–816. [PubMed: 9111219]

[29]. Kong X, Mohanty SK, Stephens J, Heale JT, Gomez-Godinez V, Shi LZ, Kim JS, Yokomori K, Berns MW, Comparative analysis of different laser systems to study cellular responses to DNA damage in mammalian cells, Nucleic Acids Res. 37 (9) (2009) 68.

[30]. Williams CG, Malik AN, Kim TK, Manson PN, Elisseeff JH, Variable cytocompatibility of six cell lines with photoinitiators used for polymerizing hydrogels and cell encapsulation, Biomaterials 26 (11) (2005) 1211–1218. [PubMed: 15475050]

[31]. Bryant SJ, Nuttelman CR, Anseth KS, Cytocompatibility of UV and visible light photoinitiating systems on cultured NIH/3T3 fibroblasts in vitro, J. Biomat Sci-Polym E 11 (5) (2000) 439–457.

[32]. Bryant SJ, Nuttelman CR, Anseth KS, Cytocompatibility of UV and visible light photoinitiating systems on cultured NIH/3T3 fibroblasts in vitro, J. Biomater. Sci. Polym. Ed 11 (5) (2000) 439–457. [PubMed: 10896041]

[33]. Prasad R, Katiyar SK, Crosstalk among UV-induced inflammatory mediators, DNA damage and epigenetic regulators facilitates suppression of the immune system, Photochem Photobiol. (2016).

[34]. Fenn SL, Oldinski RA, Visible light crosslinking of methacrylated hyaluronan hydrogels for injectable tissue repair, J. Biomed. Mater. Res. Part B, Appl. Biomater 104 (6) (2016) 1229–1236.

[35]. Fjell CD, Jenssen H, Hilpert K, Cheung WA, Pante N, Hancock RE, Cherkasov A, Identification of novel antibacterial peptides by chemoinformatics and machine learning, J. Med. Chem 52 (7) (2009) 2006–2015. [PubMed: 19296598]

[36]. Nichol JW, Koshy ST, Bae H, Hwang CM, Yamanlar S, Khademhosseini A, Cell-laden microengineered gelatin methacrylate hydrogels, Biomaterials 31 (21) (2010) 5536–5544. [PubMed: 20417964]

[37]. Raj D, Brash DE, Grossman D, Keratinocyte apoptosis in epidermal development and disease, J. Investig. Dermatol 126 (2) (2006) 243–257. [PubMed: 16418733]

[38]. Grotzinger C, Burget D, Jacques P, Fouassier JP, Visible light induced photopolymerization: speeding up the rate of polymerization by using coinitiators in dye/amine photoinitiating systems, Polymer 44 (13) (2003) 3671–3677.

[39]. Nguyen KT, West JL, Photopolymerizable hydrogels for tissue engineering applications, Biomaterials 23 (22) (2002) 4307–4314. [PubMed: 12219820]

[40]. Fouassier JP, Allonas X, Burget D, Photopolymerization reactions under visible lights: principle, mechanisms and examples of applications, Prog. Org. Coat 47 (1) (2003) 16–36.

[41]. Hao Y, Shih H, Muňoz Z, Kemp A, Lin C-C, Visible light cured thiol-vinyl hydrogels with tunable degradation for 3D cell culture, Acta biomater. 10 (1) (2014), 10.1016/j.actbio.2013.08.044.

[42]. Bahney CS, Lujan TJ, Hsu CW, Bottlang M, West JL, Johnstone B, Visible light photoinitiation of Mesenchymal stem cell-laden bioresponsive hydrogels, Eur. cells Mater 22 (2011) 43–55.

[43]. Hao Y, Shih H, Munoz Z, Kemp A, Lin CC, Visible light cured thiol-vinyl hydrogels with tunable degradation for 3D cell culture, Acta biomater. 10 (1) (2014) 104–114. [PubMed: 24021231]

[44]. Coury AJ, Philbrook CM, Skinner KC, Controlled release of anti-arrhythmic agents, Google Patents, 2004.

[45]. Li C, Guan G, Reif R, Huang Z, Wang RK, Determining elastic properties of skin by measuring surface waves from an impulse mechanical stimulus using phase-sensitive optical coherence tomography, J. R. Soc. Interface 9 (70) (2012) 831–841. [PubMed: 22048946]

[46]. Shevchenko RV, James SL, James SE, A review of tissue-engineered skin bioconstructs available for skin reconstruction, J. R. Soc. Interface 7 (43) (2010) 229–258. [PubMed: 19864266]

[47]. Skotheim TA, Reynolds JR, Handbook of Conducting Polymers. Conjugated polymers: theory, Synthesis, Properties, and Characterization, third ed., CRC Press, Boca Raton, 2007.

[48]. Perez RA, Kim H-W, Ginebra M-P, Polymeric additives to enhance the functional properties of calcium phosphate cements, J. Tissue Eng 3 (1) (2012), 2041731412439555. [PubMed: 22511991]

[49]. Park SC, Park Y, Hahm KS, The role of antimicrobial peptides in preventing multidrug-resistant bacterial infections and biofilm formation, Int. J. Mol. Sci 12 (9) (2011) 5971–5992. [PubMed: 22016639]

[50]. Annabi N, Nichol JW, Zhong X, Ji C, Koshy S, Khademhosseini A, Dehghani F, Controlling the porosity and microarchitecture of hydrogels for tissue engineering, Tissue Eng. Part B Rev 16 (4) (2010) 371–383. [PubMed: 20121414]

[51]. Peppas NA, Hilt JZ, Khademhosseini A, Langer R, Hydrogels in biology and medicine: from molecular principles to bionanotechnology, Adv. Mater 18 (11) (2006) 1345–1360.

[52]. Kumar PTS, Lakshmanan VK, Biswas R, Nair SV, Jayakumar R, Synthesis and biological evaluation of chitin hydrogel/nano ZnO composite bandage as antibacterial wound dressing, J. Biomed. Nanotechnol 8 (6) (2012) 891–900. [PubMed: 23029997]

[53]. Duarte AP, Coelho JF, Bordado JC, Cidade MT, Gil MH, Surgical adhesives: systematic review of the main types and development forecast, Prog. Polym. Sci 37 (8) (2012) 1031–1050.

[54]. A. F2255-05(2015), Standard test method for strength properties of tissue adhesives in lap-shear by tension loading, ASTM Int. 13 (01) (2015).

[55]. Sierra DH, Feldman DS, Saltz R, Huang S, A method to determine shear adhesive strength of fibrin sealants, J. Appl. Biomater 3 (2) (1992) 147–151. [PubMed: 10147711]

[56]. Annabi N, Tamayol A, Shin SR, Ghaemmaghami AM, Peppas NA, Khademhosseini A, Surgical materials: current challenges and nano-enabled solutions, Nano Today 9 (5) (2014) 574–589. [PubMed: 25530795]

[57]. A. F2392–04(2015), Standard test method for burst strength of surgical sealants, ASTM Int. 13 (01) (2015).

[58]. A. F2458–05(2015), Standard test method for wound closure strength of tissue adhesives and sealants, ASTM Int. 13 (01) (2015).

[59]. Lang N, Pereira MJ, Lee Y, Friehs I, Vasilyev NV, Feins EN, Ablasser K, O'Cearbhaill ED, Xu C, Fabozzo A, Padera R, Wasserman S, Freudenthal F, Ferreira LS, Langer R, Karp JM, del Nido PJ, A blood-resistant surgical glue for minimally invasive repair of vessels and Heart defects, Sci. Transl. Med 6 (218) (2014) 218ra6.

[60]. Yao M, Yaroslavsky A, Henry FP, Redmond RW, Kochevar IE, Phototoxicity is not associated with photochemical tissue bonding of skin, Lasers Surg. Med 42 (2) (2010) 123–131. [PubMed: 20166159]

[61]. Smart JD, The basics and underlying mechanisms of mucoadhesion, Adv. drug Deliv. Rev 57 (11) (2005) 1556–1568. [PubMed: 16198441]

[62]. Chellat MF, Raguz L, Riedl R, Targeting antibiotic resistance, Angew. Chem. Int. Ed. Engl 55 (23) (2016) 6600–6626. [PubMed: 27000559]

[63]. Shi J, Liu Y, Wang Y, Zhang J, Zhao S, Yang G, Biological and immunotoxicity evaluation of antimicrobial peptide-loaded coatings using a layer-by-layer process on titanium, Sci. Rep 5 (2015) 16336. [PubMed: 26548760]

[64]. Hale JD, Hancock RE, Alternative mechanisms of action of cationic antimicrobial peptides on bacteria, Expert Rev. Anti Infect. Ther 5 (6) (2007) 951–959. [PubMed: 18039080]

[65]. Silva JP, Dhall S, Garcia M, Chan A, Costa C, Gama M, Martins-Green M, Improved burn wound healing by the antimicrobial peptide LLKKK18 released from conjugates with dextrin embedded in a carbopol gel, Acta biomater. 26 (2015) 249–262. [PubMed: 26234490]

[66]. Babavalian H, Latifi AM, Shokrgozar MA, Bonakdar S, Mohammadi S, Moosazadeh Moghaddam M, Analysis of healing effect of alginate sulfate hydrogel dressing containing antimicrobial peptide on wound infection caused by methicillin-resistant Staphylococcus aureus, Jundishapur J. Microbiol 8 (9) (2015) 28320.

[67]. Boulos L, Prevost M, Barbeau B, Coallier J, Desjardins R, LIVE/DEAD BacLight : application of a new rapid staining method for direct enumeration of viable and total bacteria in drinking water, J. Microbiol. Methods 37 (1) (1999) 77–86. [PubMed: 10395466]

[68]. Madhumitha G, Elango G, Roopan SM, Biotechnological aspects of ZnO nanoparticles: overview on synthesis and its applications, Appl. Microbiol. Biotechnol 100 (2) (2016) 571–581. [PubMed: 26541334]

[69]. Oyarzun-Ampuero F, Vidal A, Concha M, Morales J, Orellana S, Moreno-Villoslada I, Nanoparticles for the treatment of wounds, Curr. Pharm. Des 21 (29) (2015) 4329–4341. [PubMed: 26323420]

[70]. Chevallet M, Gallet B, Fuchs A, Jouneau PH, Um K, Mintz E, Michaud-Soret I, Metal homeostasis disruption and mitochondrial dysfunction in hepatocytes exposed to sub-toxic doses of zinc oxide nanoparticles, Nanoscale 8 (43) (2016) 18495–18506. [PubMed: 27782264]

[71]. Bostan HB, Rezaee R, Valokala MG, Tsarouhas K, Golokhvast K, Tsatsakis AM, Karimi G, Cardiotoxicity of nano-particles, Life Sci. 165 (2016) 91–99. [PubMed: 27686832]

[72]. Chen S, Shi J, Zhang M, Chen Y, Wang X, Zhang L, Tian Z, Yan Y, Li Q, Zhong W, Xing M, Zhang L, Zhang L, Mesenchymal stem cell-laden anti-inflammatory hydrogel enhances diabetic wound healing, Sci. Rep 5 (2015) 18104. [PubMed: 26643550]

[73]. Dreesmann L, Ahlers M, Schlosshauer B, The pro-angiogenic characteristics of a cross-linked gelatin matrix, Biomaterials 28 (36) (2007) 5536–5543. [PubMed: 17889331]

[74]. Wang Y, Mithieux SM, Kong Y, Wang X-Q, Chong C, Fathi A, Dehghani F, Panas E, Kemnitzer J, Daniels R, Kimble RM, Maitz PK, Li Z, Weiss AS, Tropoelastin incorporation into a dermal

regeneration template promotes wound angiogenesis, Adv. Healthc. Mater 4 (4) (2015) 577–584. [PubMed: 25469903]

[75]. Boddupalli A, Zhu L, Bratlie KM, Methods for implant acceptance and wound healing: material selection and implant location modulate macrophage and fibroblast phenotypes, Adv. Healthc. Mater 5 (20) (2016) 2575–2594. [PubMed: 27593734]

[76]. Wende FJ, Gohil S, Nord LI, Helander Kenne A, Sandström C, 1D NMR methods for determination of degree of cross-linking and BDDE substitution positions in HA hydrogels, Carbohydr. Polym 157 (2017) 1525–1530. [PubMed: 27987864]

[77]. Annabi N, Shin SR, Tamayol A, Miscuglio M, Bakooshli MA, Assmann A, Mostafalu P, Sun JY, Mithieux S, Cheung L, Tang XS, Weiss AS, Khademhosseini A, Highly elastic and conductive human-based protein hybrid hydrogels, Adv. Mater 28 (1) (2016) 40–49. [PubMed: 26551969]

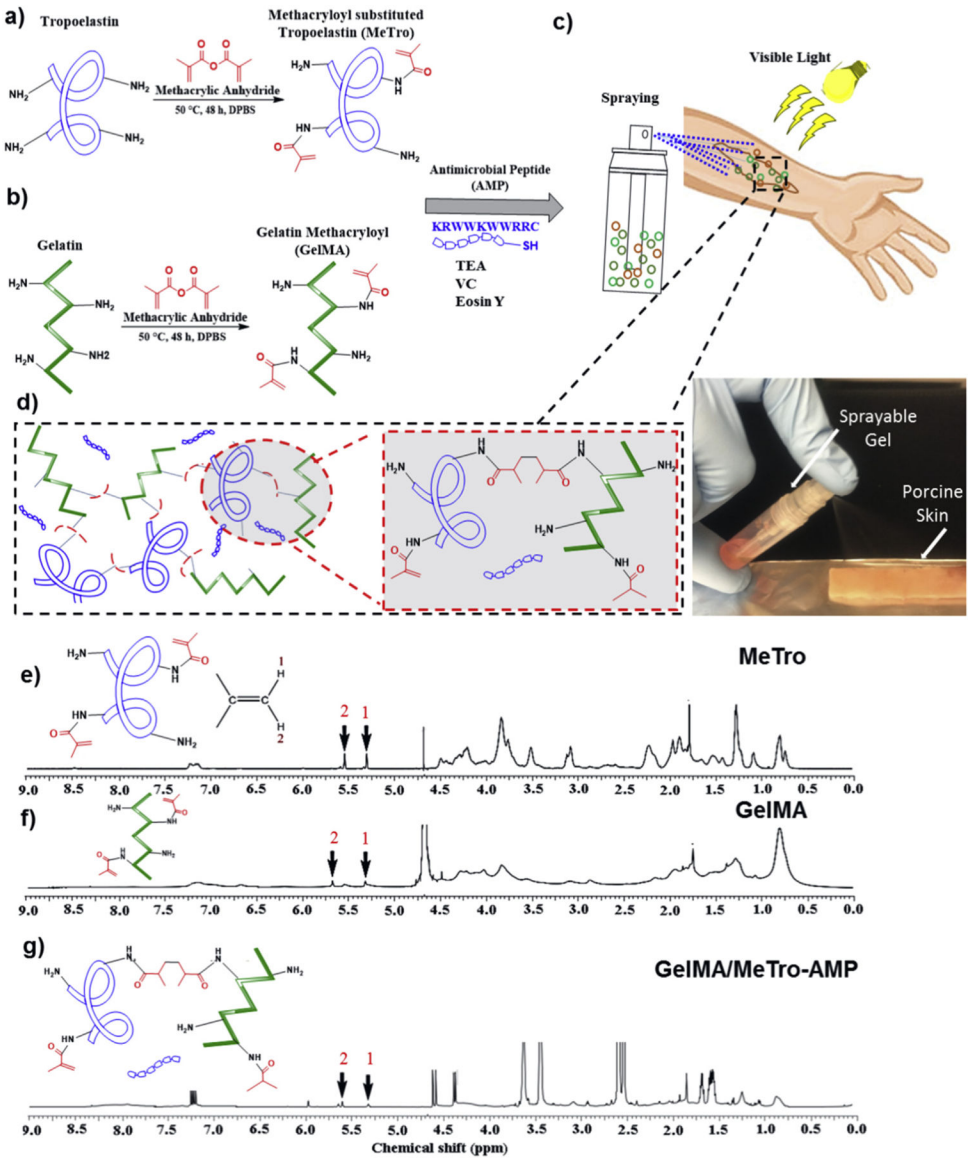

Fig. 1. Synthesis and ^{1}H NMR analysis of MeTro/GelMA-AMP composite hydrogels.

Design and photocrosslinking of composite hydrogels. The panel shows a schematic of the proposed reaction for synthesis of **(a)** MeTro, and **(b)** GelMA, and **(c–d)** MeTro-GelMA-AMP; AMP, GelMA, and MeTro were added in a TEA (co-initiator) and VC (co-initiator) solution. Immediately prior to photocrosslinking, Eosin Y (photoinitiator) was introduced into the solution. The solution could be sprayed onto a wound area and exposed to visible light to form an adhesive and elastic antimicrobial hydrogel layer. ^{1}H NMR (500 MHz; D_2O) spectra of **(e)** MeTro prepolymer, **(f)** GelMA prepolymer, and **(g)** MeTro/GelMA-AMP hydrogels.

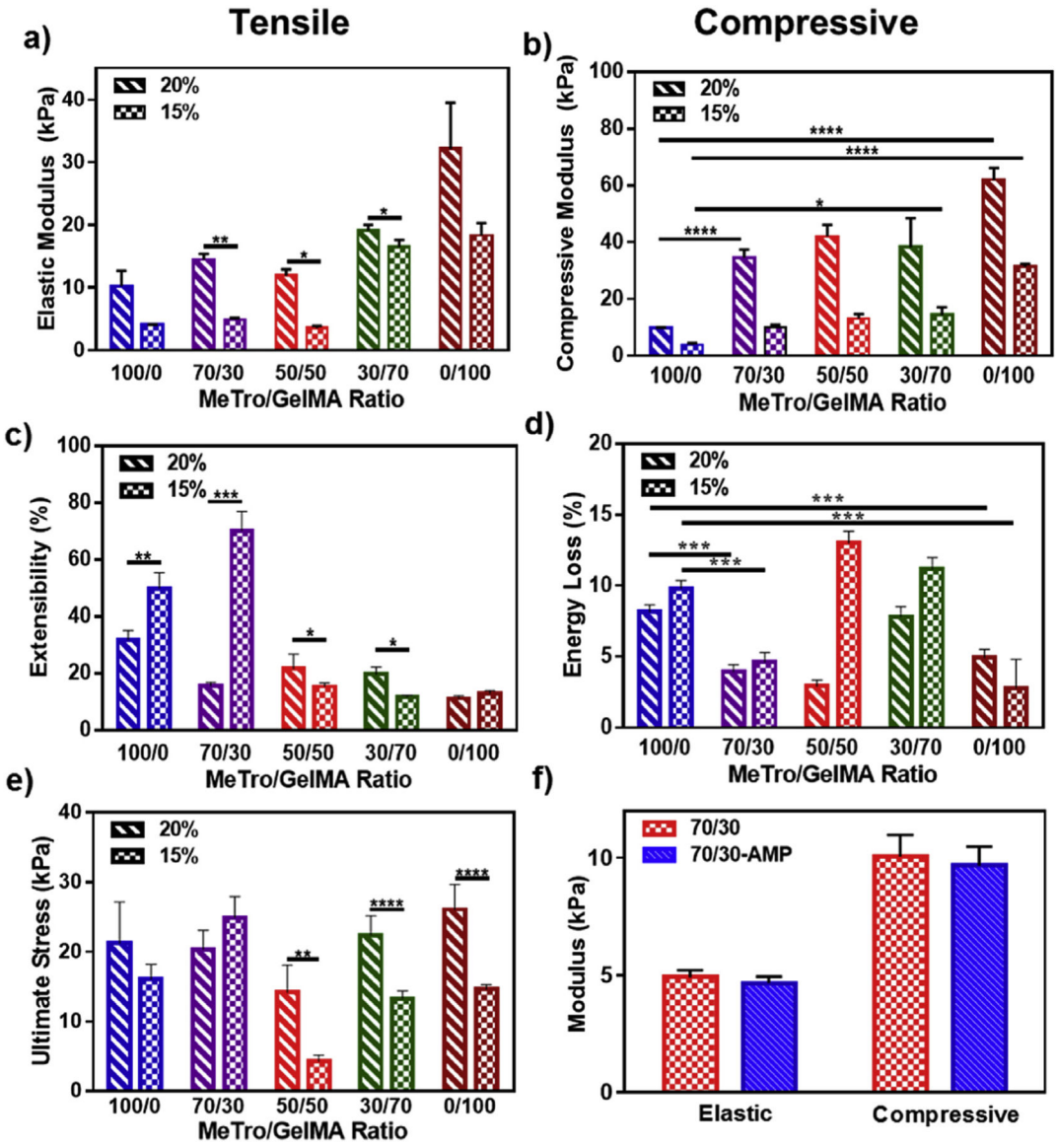

Fig. 2. Mechanical characterization of MeTro/GelMA and MeTro/GelMA-AMP composite hydrogels.

(a) Elastic modulus, **(b)** compressive modulus, **(c)** extensibility, **(d)** energy loss, and **(e)** ultimate stress of hydrogels produced by using 15% and 20% (w/v) total polymer concentration, at varying ratios of MeTro to GelMA. **(f)** Elastic and compressive modulus of MeTro/GelMA and MeTro/GelMA-AMP (containing 0.1% (w/v) AMP) hydrogels produced by using 15% (w/v) total polymer concentration; the results show no significant difference in mechanical properties of hydrogels with and without AMP. Data is represented as mean ± SD (*$p < 0.05$, **$p < 0.01$, ***$p < 0.001$, ****$p < 0.0001$ and $n \geq 5$).

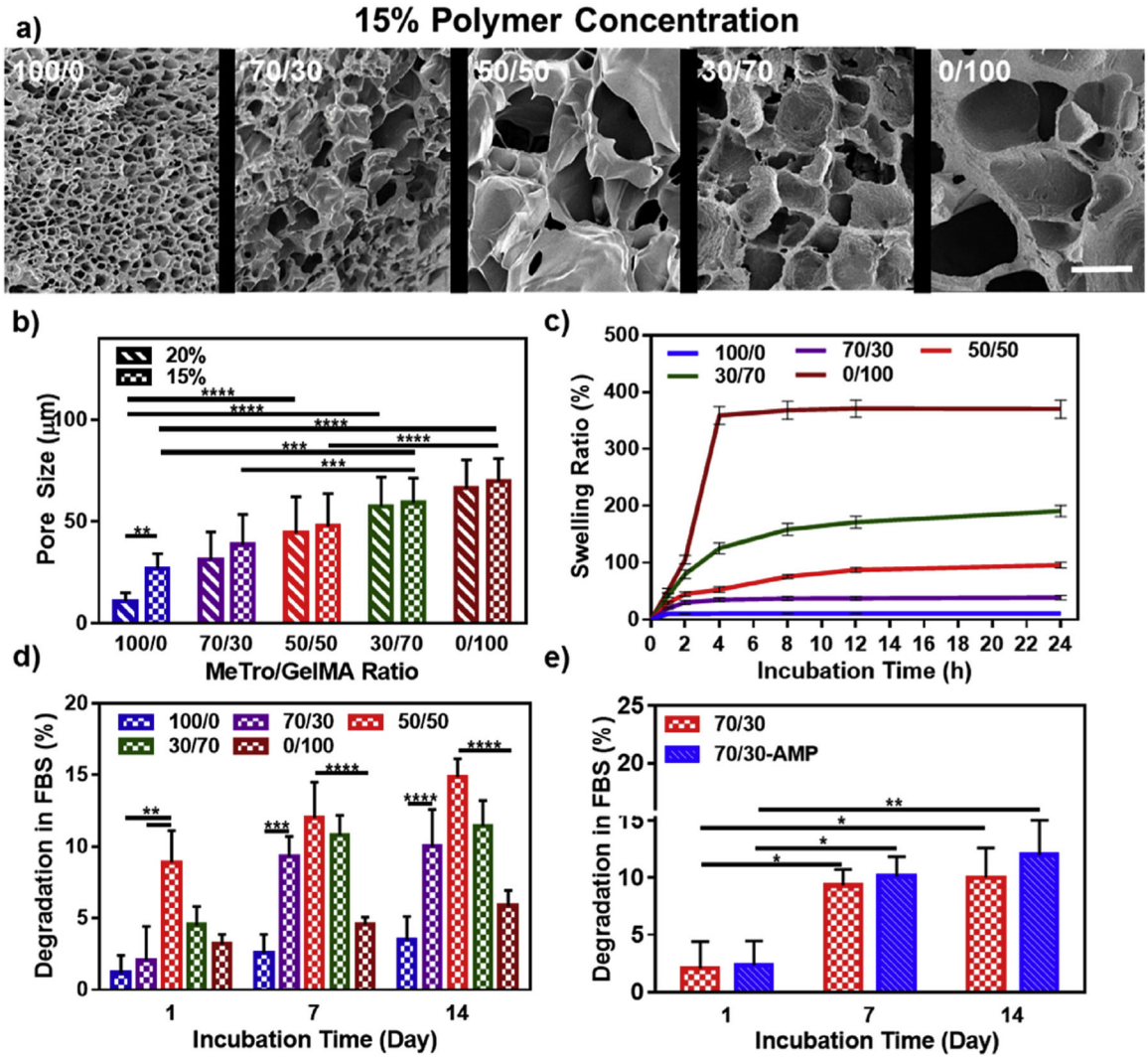

Fig. 3. Pore characteristics, swelling ratios and *in vitro* degradation properties of MeTro/GelMA composite hydrogels.

(a) Representative SEM images and **(b)** pore size characterization of MeTro/GelMA composite hydrogels at varying MeTro/GelMA ratios and 15% final polymer concentration (scale bar = 100 μm). **(c)** Swelling ratios (in DPBS) and **(d)** degradation properties (in DPBS+10% FBS solution) of 15% composite hydrogels at varying ratios of MeTro/GelMA at 37 °C. **(e)** *In vitro* degradation of MeTro/GelMA and MeTro/GelMA-AMP (containing 0.1% (w/v) AMP) hydrogels at 15% (w/v) total polymer concentration and 70/30 MeTro/GelMA ratio; the results show no significant difference in degradation properties of hydrogels with and without AMP. Data is represented as mean ± SD (*$p < 0.05$, **$p < 0.01$, ***$p < 0.001$, ****$p < 0.0001$ and $n \geq 5$).

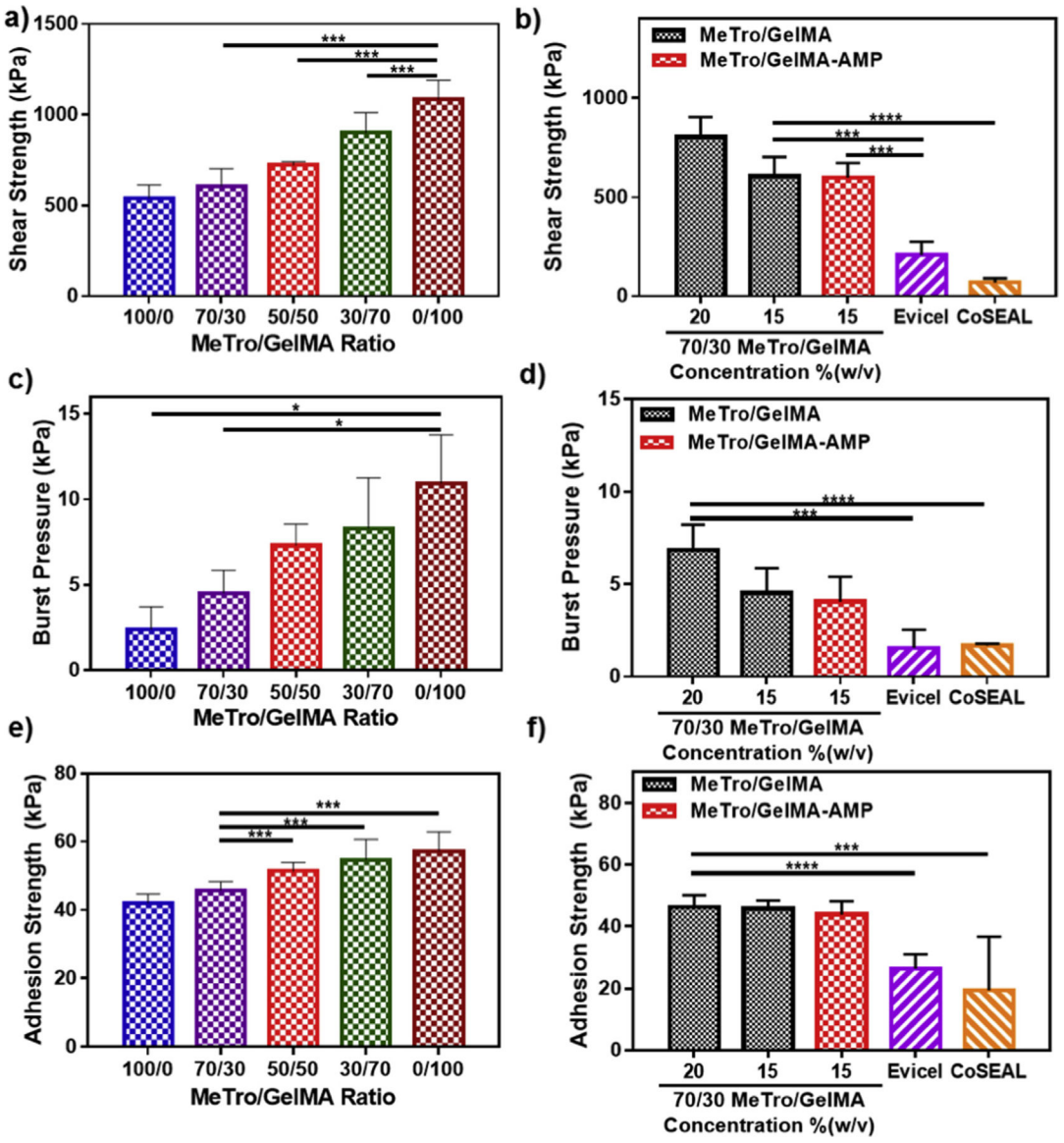

Fig. 4. ***In vitro*** **adhesion properties of MeTro/GelMA composite hydrogels.**

The *in vitro* shear strength of **(a)** composite hydrogels at varying MeTro/GelMA ratios and 15% polymer concentration, and **(b)** 70/30 MeTro/GelMA hydrogels at 20% and 15% polymer concentrations with and without AMP and different commercially available adhesives (Evicel and Coseal). The *in vitro* burst pressure of composite hydrogels at **(c)** varying MeTro/GelMA ratios and 15% polymer concentration, and **(d)** 70/30 MeTro/GelMA hydrogels at 20% and 15% polymer concentrations with and without AMP and different commercially available adhesives (Evicel and Coseal). The *in vitro* adhesion strength of composite hydrogels at **(e)** varying MeTro/GelMA ratios and 15% polymer concentration, and **(f)** 70/30 MeTro/GelMA hydrogels at 20% and 15% polymer concentrations with and without AMP and different commercially available adhesives (Evicel and Coseal). Data is represented as mean ± SD (*$p < 0.05$, **$p < 0.01$, ***$p < 0.001$, ****$p < 0.0001$, $n \geq 5$).

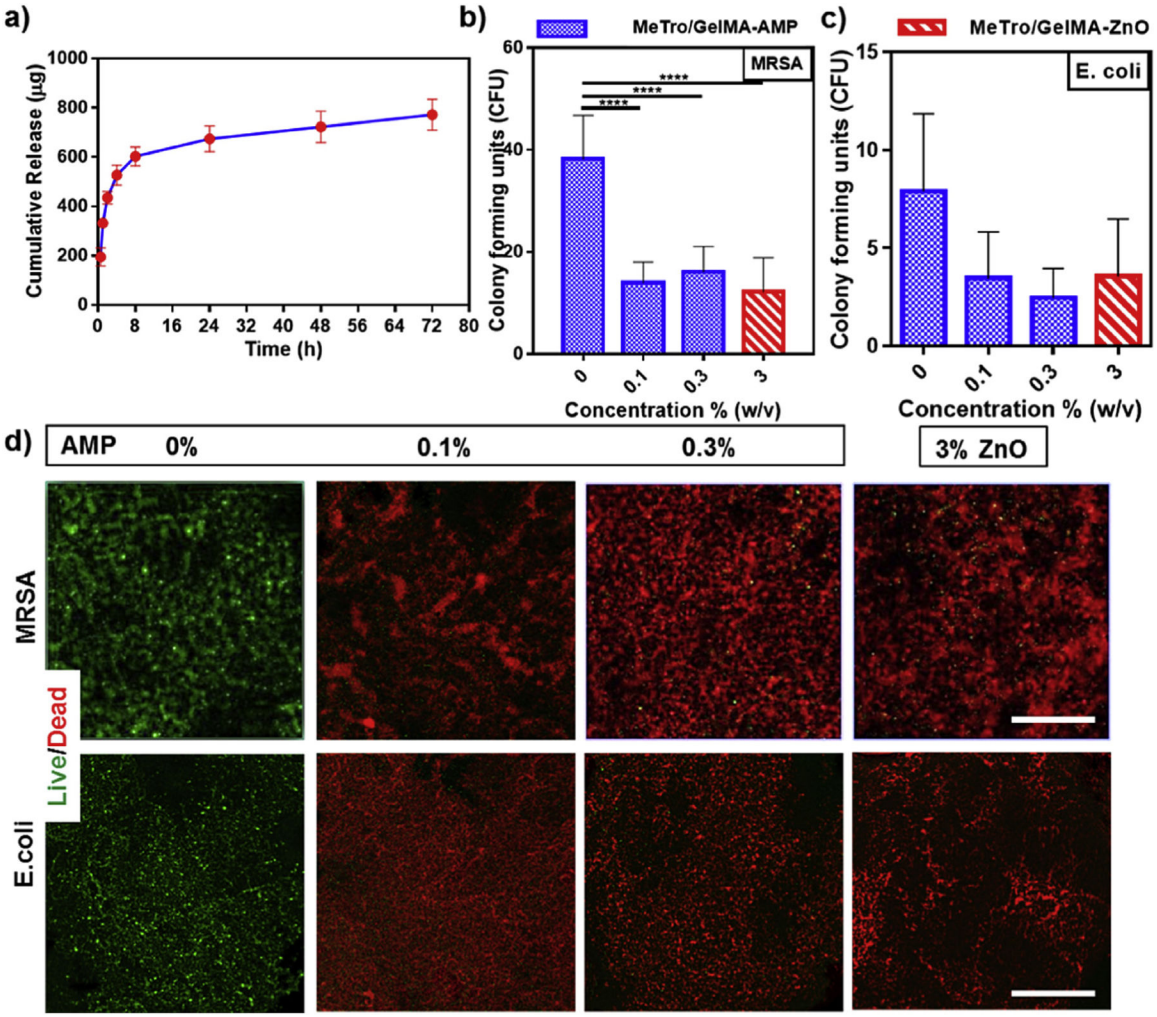

Fig. 5. ***In vitro*** **AMP release profile and antibacterial properties of Metro/GelMA-AMP hydrogels as compared to MeTro/GelMA (control) and Metro/GelMA-ZnO hydrogels.**

(a) *In vitro* release profile of AMP from 70/30 MeTro/GelMA-AMP hydrogels at 15% (w/v) total polymer concentration. Colony forming units test for MeTro/GelMA-AMP hydrogels with different AMP content (0% as a control, 0.1% and 0.3% (w/v)) and 3% (w/v) ZnO nanoparticles seeded with **(b)** methicillin-resistant *S aureus* (MRSA) and **(c)** *E. coli*. **(d)** Representative live/dead images from MRSA and *E. coli* seeded on MeTro/GelMA-AMP hydrogels with different AMP content (0% as a control, 0.1% and 0.3% (w/v)) and 3% (w/v) ZnO nanoparticles. (Scale bar = 200 µm). Data is represented as mean ± SD (*$p < 0.05$, **$p < 0.01$, ***$p < 0.001$, ****$p < 0.0001$, $n \geq 3$).

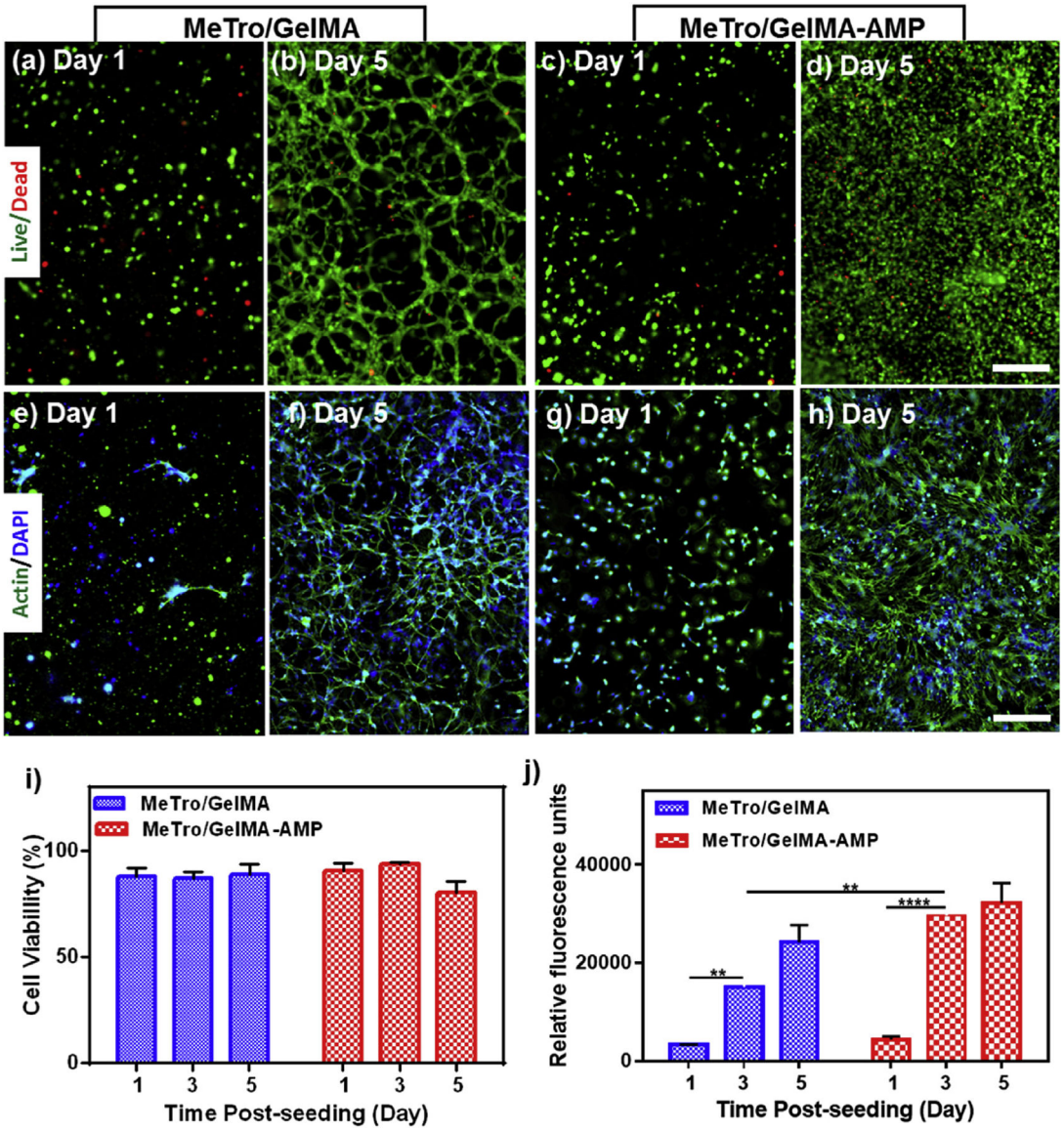

Fig. 6. ***In vitro*** **3D cell encapsulation in MeTro/GelMA and MeTro/GelMA-AMP (0.1% (w/v) AMP) hydrogels using 3T3 cells.**

Representative live/dead images from 3T3 encapsulated within the **(a–b)** MeTro/GelMA **(c–d)** and MeTro/GelMA-AMP hydrogels on days 1 and 5. Representative Actin/DAPI stained images for 3T3 cells encapsulated within **(e–f)** MeTro/GelMA **(g, h)** and MeTro/GelMA-AMP hydrogels on days 1 and 5 (scale bar = 200 μm). **(i)** Quantification of cell viability encapsulated in MeTro/GelMA and MeTro/GelMA-AMP hydrogels after 1, 3, and 5 days of encapsulation. **(j)** Quantification of metabolic activity of 3T3 cells encapsulated in MeTro/GelMA and MeTro/GelMA-AMP hydrogels after 1, 3, and 5 days. 30/70 MeTro/GelMA hydrogels at 10% (w/v) total polymer concentration were used for 3D cell encapsulation. Data is represented as mean ± SD (*$p < 0.05$, **$p < 0.01$, ***$p < 0.001$ and ****$p < 0.0001$, $n \geq 3$).

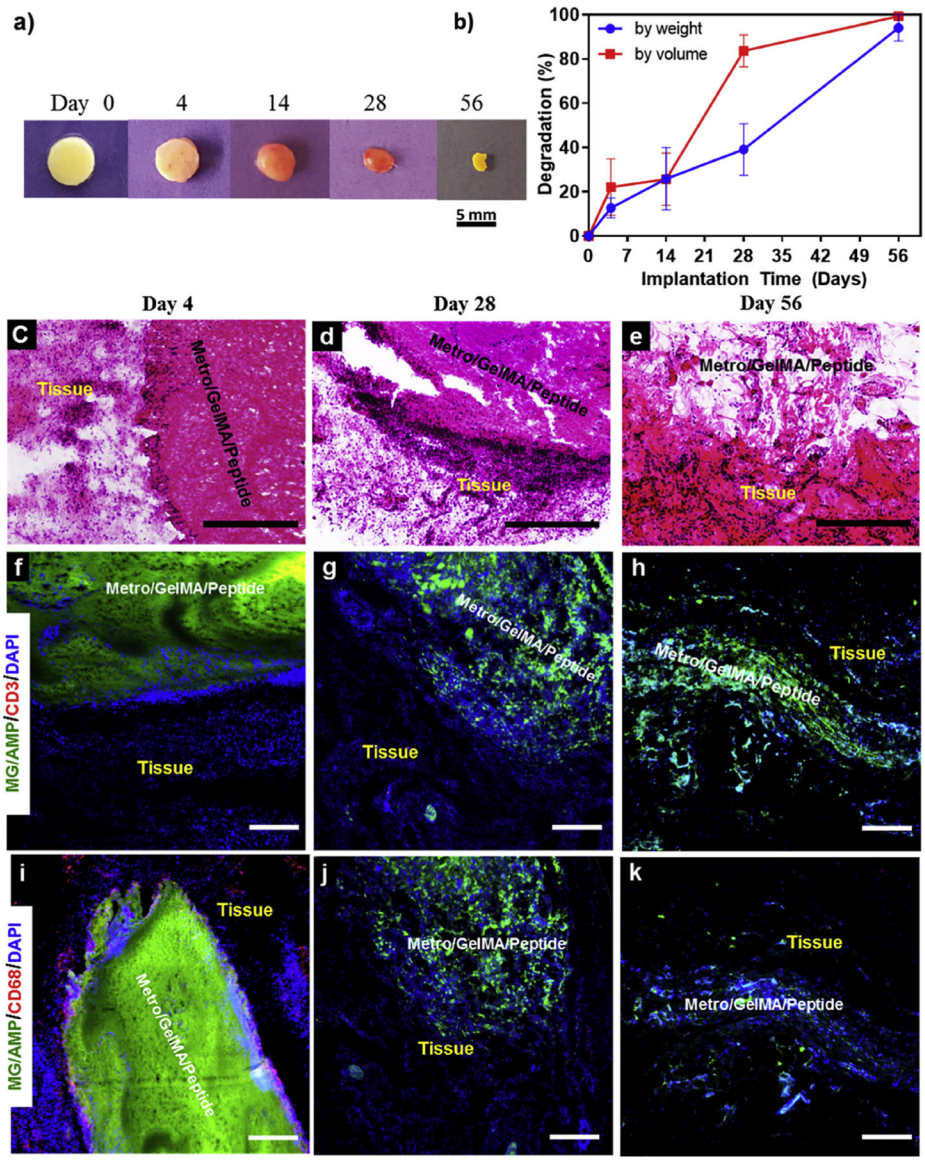

Fig. 7. ***In vivo*** **biocompatibility and biodegradation of MeTro/GelMA-AMP composite hydrogel using a rat subcutaneous model.**

(a) Representative images of the MeTro/GelMA-AMP hydrogels before implantation (Day 0) and on days 4, 14, 28, 56 post-implantation. **(b)** *In vivo* biodegradation of MeTro/GelMA-AMP hydrogels on days 0, 4, 14, 28 and 56 of implantation (n = 4). Hematoxylin and eosin (H&E) staining of MeTro/GelMA-AMP sections (hydrogels with the surrounding tissue) after **(c)** 4 days, **(d)** 28 days, and **(e)** 56 days of implantation (scale bars = 500 μm). (c) Fluorescent immunohistochemical analysis of subcutaneously implanted MeTro/GelMA-AMP hydrogels showing no significant local lymphocyte infiltration (CD3) at days **(f)** 4, **(g)** 28 and **(h)** 56 (scale bars = 200 μm), and exhibiting macrophages (CD68) at **(i)** day 4 but not at days **(j)** 28 and **(k)** 56 (scale bars = 200 μm). Green, red and blue colors in (**f–k**) represent the MeTro/GelMA-AMP hydrogels, the immune cells, and the cell nuclei (DAPI)

respectively. 50/50 MeTro/GelMA hydrogels at 15% (w/v) total polymer concentration were used for the *in vivo* test.